# Conditions for organized nanoring growth using kinetic Monte Carlo simulations

F. Dumont, F. Picaud, C. Ramseyer, and C. Girardet
*Laboratoire de Physique Moléculaire, UMR CNRS 6624, Faculté des Sciences, La Bouloie, Université de Franche-Comté, F25030 Besançon Cedex, France*

(Received 11 January 2008; published 4 April 2008)

Kinetic Monte Carlo simulations are carried out to analyze the conditions for the occurrence of organized nanorings in heteroepitaxy by alternatively depositing two different atomic species on a perfect surface. We demonstrate that drastic conditions are required on the flux and substrate temperature and on the activation barriers of the species including their environment to provide such organized nanostructures. These constraints come from the competition between flux and diffusion along island edges on the one hand and between flux and intermixing on the other hand.

DOI: 10.1103/PhysRevB.77.153404 PACS number(s): 81.15.−z, 02.70.−c, 66.70.Df, 79.60.Jv

Since progress in the fields of electronic and optical devices relies on their miniaturization, great efforts have been done to fabricate nanosized epitaxial structures as quantum dots[1–6] or nanowires[7,8] on surfaces. Heteroepitaxy has been widely studied to define, through various models,[9–17] the conditions of formation of self-organized nanostructures regarding their number, size, shape, and chemical composition. Carefully controlling and monitoring the size and geometry of these structures generate specific electric,[18] optical,[19] and magnetic[20] properties. Although the role of a surfactant in the heteroepitaxial growth has been largely analyzed, there are still unresolved issues.[21] Controlled deposition of Ge on Si(111) with Bi as a surfactant has been recently used as an experimental model system to understand the growth mechanism of islands[22–24] on the surface and to fabricate alternating Si/Ge nanowires[7,8] and nanorings[7,25] of one atomic layer height. Awkwardly, the experimental conditions for obtaining such nanoring arrays are packed in a narrow window and, to our knowledge, restricted to this specific system.

Therefore, questions arise about (i) the general nature of the phenomenon and (ii) the drastic conditions required to reach sequentially well-organized rings. As far as equilibrium states are deeply involved, kinetic Monte Carlo is a relevant tool to drive theoretical work.[26] This Brief Report is another attempt to interpret the nanoring occurrence. The solid-on-solid[9,10] model is simple enough to allow a general relevance for metals and semiconductors and to predict the subtle conditions leading to the formation of epitaxial nanorings. It has been proved for a long time that it is efficient to understand the salient features of growth kinetics in homoepitaxy.[27,28] In heteroepitaxial systems, the lattice mismatch can induce strains and may cause other types of changes.[29] To analyze the effect of this mismatch, improvements in the initial solid-on-solid model have been provided by using elasticity principles. In particular, a harmonic approach has been proposed where lattice sites are connected by springs to allow for the lattice deformation.[30–32] Such an improvement has not been taken into account here, meaning that the present model is available when the size of deposited atoms is reasonably consistent with the size of the host surface sites. Despite this simple approach, we show in this Brief Report that we can identify the main causes of ring formation.

The simulations start on a perfect surface with square symmetry at temperature $T$, in which atomic species $A$ and $B$ are deposited with respective fluxes $F_A$ and $F_B$ at the top of the squares. Desorption is forbidden, and at low coverage [$\theta \leq 0.3$ ML (nanolayer)], second layer nucleation is disregarded. This latter assumption is consistent with the fact that surfactant can act as an inhibitor of three-dimensional growth. Migration occurs through nearest neighbor hopping processes following an Arrhenius law. For an atom $X$ ($X=A$ or $B$), the hopping rate is $R_D^X = \nu_D \exp(-E_D^X/k_BT)$, where $\nu_D = 2\times 10^{12}$ Hz is commonly used for the attempt frequency of an adatom on the surface and $k_BT$ is the thermal energy. The hopping barrier $E_D^X$ is

$$E_D^X = E_D^X(0) + n_X E_{XX} + n_Y E_{XY}, \tag{1}$$

where $E_D^X(0)$ is the diffusion barrier of an atom $X$ without neighbors and $n_X$ and $n_Y$ represent the number of atoms which are nearest neighbor of diffusing atoms $X$ and $Y$, respectively. $E_{XX}$ and $E_{XY}=E_{YX}$ are the interactions between two $X$ atoms and two atoms $X$ and $Y$. An additional process describes the intermixing[10,33] between $A$ and $B$ species, via the exchange process between two different nearest neighbor atoms, thermally activated with a rate $R_M=\nu_M \exp(-E_M/k_BT)$. We assume that $\nu_M=\nu_D$, and the activation energy for the mixing process is

$$E_M = E_M(0) + (m_{AA} - m'_{AA})E_{AA} + (m_{AB} - m'_{AB})E_{AB} + (m_{BB} - m'_{BB})E_{BB}, \tag{2}$$

where $E_M(0)$ is the mixing barrier of a pair $AB$ without neighbors and $m_{XY}$ and $m'_{XY}$ represent the number of nearest neighbor bonds of type $XY$ around the exchanging pair before and after the process, respectively.

The two species $A$ and $B$ are sequentially deposited. On the $200\times 200$ surface with periodic conditions, 0.05 ML of $A$ atoms is first deposited, then 0.10 ML of $B$, and finally 0.15 ML of $A$, in order to reach regular thickness of the desired rings, at the final coverage $\theta=0.3$ ML. The flux $F$, assumed to be identical to the two species, is varied from $10^{-3}$ to 1 ML $s^{-1}$. We use a generic set of parameter characteristics of metals, with $E_D^B(0)=E_D^A(0)\equiv E_D=0.2$ eV, and $E_M(0)=2E_D$. In addition, we assume that $E_{AA}=E_{BB}=E_{AB}\equiv E_L=E_D/2$. We will note $E_D$ and $E_L$ to be the respective common diffusion barrier and lateral energy.

Figure 1 shows a regular array of nanoringed islands obtained at $T=135$ K and $F=0.02$ ML $s^{-1}$. Although these con-

 

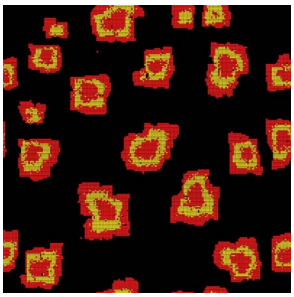

FIG. 1. (Color online) Example of nanoring array on a 200 $\times$200 periodic surface at the final coverage $\theta$=0.3 ML at $T$ =135 K, obtained by successive deposition of 0.05 ML of $A$, 0.10 ML of $B$, and again 0.15 ML of $A$, with a flux $F$=0.02 ML s$^{-1}$, diffusion barrier $E_D$=0.2 eV, lateral interaction $E_L$=0.1 eV, and mixing barrier $E_M(0)$=0.4 eV.

ditions lead to island sizes about six times smaller than in experiments[7,25] (this way is necessary to save computation time), qualitative arguments remain valid. The islands grow with different sizes as expected from the behavior of a single adspecies.[34,35] However, the morphologies are very similar from one island to another, except for a few (smaller) clusters formed after secondary nucleation of $B$, in depleted zones remaining after primary nucleation of $A$. This leads to mixing that sharpens the ring edges, which is nevertheless insufficient to create completely alloyed islands. We can then see (Fig. 1) that the island shape and ring thickness are directly linked to the Voronoï zone surrounding each island.

Figure 2 displays the influence of the temperature on the island morphology at fixed value of the flux $F$ =0.02 ML s$^{-1}$. The chemical composition of a four atom wide band, here and there around the green line representing the largest size of a selected island in Figs. 2(b)–2(e), was analyzed. For each row of atoms perpendicular to the line, the number of $A$ and $B$ atoms was counted. The curves at the right hand side of Fig. 2 display the percentage of each species and their sum. As expected, island size increases with temperature, and island density decreases while the island shapes become smoother. At $T$=120 K [Fig. 2(a)], the fractal-to-compact transition[36] is not complete, island shapes remain fractal-like, and ring formation does not occur. An increase in $T$ activates diffusion around existing clusters, leading to reorganization of cluster sides. Hence, rings are formed at $T\approx$130 K [Fig. 2(b)]. As temperature still increases, intermixing is activated, as shown in Fig. 2(c), where we can see some $A$-type atoms marooned in $B$ zones and reciprocally. At $T$=150 K, Fig. 2(d) exhibits hazy rings, and when $T$ reaches 160 K, alloyed islands are obtained [Fig. 2(e)]. More precisely, the core of the islands is totally mixed, while the edges mainly formed by $A$ species remain. This is not surprising because the edge atoms had just been deposited (species $A$) and stuck to the islands at the very end of the simulation. The higher the temperature is, the thinner the $A$-type border is, and the more it is mixed. We can finally note that, as $T$ increases, the island edge reorganization progressively becomes efficient, leading to a regular island geometry. The first step in this way was diffusion along a linear edge due to a reduced mobility at the island border. Thus, the edge growth is directly related to the shape of its Voronoï

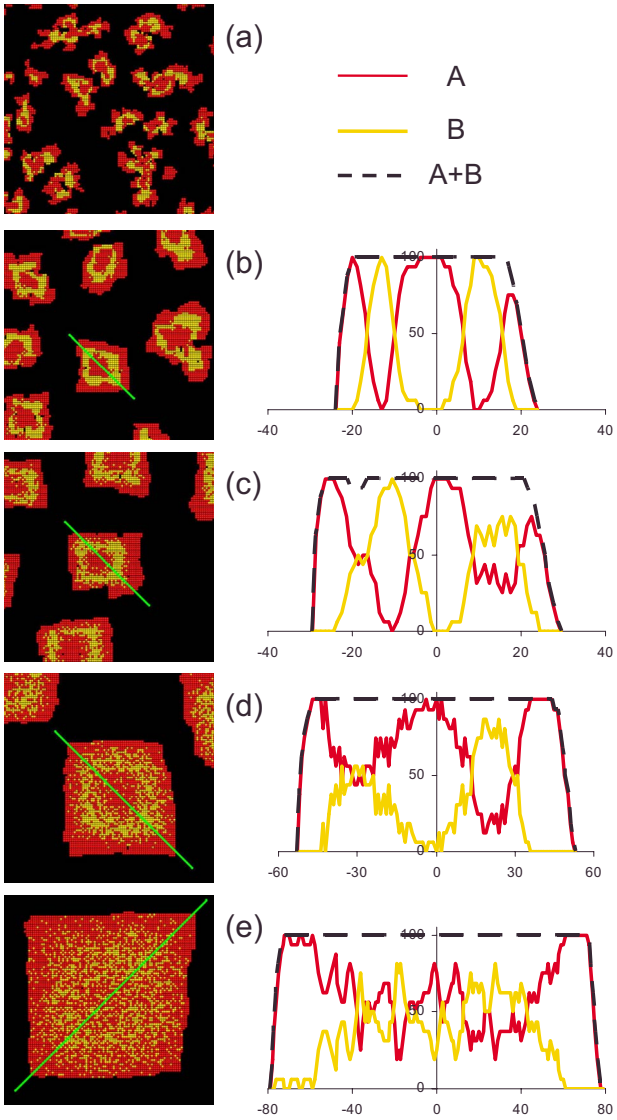


FIG. 2. (Color online) Result of the simulations at the final coverage $\theta$=0.3 ML [same conditions as in Fig. 1] for various substrate temperatures (a) $T$=120 K, (b) $T$=130 K, (c) $T$=140 K, (d) $T$=150 K, and (e) $T$=160 K. Left: only 100$\times$100 sections of the simulation box are shown. Right: behavior of the chemical composition of the islands along the green lines drawn on the images. The horizontal scale defines the size of the island along this line, reduced by the lattice parameter. The broken curves are the sum of the two species number in percent unit.

zone. In the second step [Figs. 2(d) and 2(e)], diffusion around corners and kinks is favored, and the islands progressively reach their equilibrium square shapes, consistent with the surface geometry.

Figure 3 describes the mean number of bonds per atom [Fig. 3(a)] and the percentage of $A$-$A$, $B$-$B$, and mixed $A$-$B$ bonds [Fig. 3(b), solid lines] as a function of temperature. At low temperature, atoms are randomly deposited on the surface and diffusion is hindered. The number of bonds depends on the partial coverages of $A$ and $B$ only. As $T$ increases, an organization of the species proceeds, forming fractal islands, which increases the global coordination number [Fig. 3(a)], but does not modify the statistical repartition of the bonds

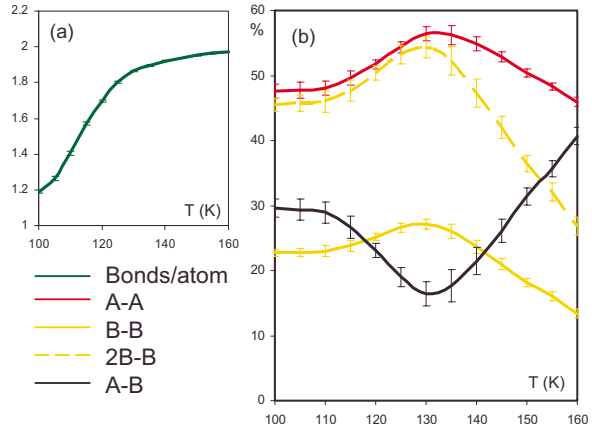


FIG. 3. (Color online) Mean number of bonds per atom at final coverage $\theta$=0.3 ML vs the substrate temperature. (a) Total number of bonds. (b) Percentages of *A*-*A*, *B*-*B*, and mixed *A*-*B* bonds (solid lines); the percentage of *B*-*B* bonds is doubled (broken line) to be directly compared to the percentage of *A*-*A* bonds (see the text). The vertical error bars estimate the standard deviation over ten independent runs.

until $T$=110 K [Fig. 3(b)]. Between 110 and 125 K, the compact-to-fractal transition occurs, with an increase in the island dimension from $d_f \approx 1.7$ to 2. The perimeter over surface ratio of the islands and the corresponding number of dangling bonds drastically diminish, leading to a strong increase in the bond number [Fig. 3(a)]. As the regular ring shape appears, the zones of *A* and *B* species are compact, and their interface is reduced. As a result, the number of mixed *A*-*B* bonds decreases, while that of bulk *A*-*A* and *B*-*B* bonds increases [Fig. 3(b)]. In order to directly compare the organization of *A* and *B* species, the number of bonds was normalized to the partial coverages of *A* and *B* species (remember that $\theta_A = 2\theta_B$). The broken curve in Fig. 3(b) takes into account this correction in the percentage of *B*-*B* bonds. It shows that until $T$=130 K, the number of *A*-*A* and *B*-*B* bonds is proportional to their partial coverage and merely follows the same behavior [Fig. 3(b)]. This mainly characterizes the compact zones of both *A* and *B*, the *A*-*B* bonds being significant at the interface, only. On the contrary, at higher $T$ (over 130 K), mixing occurs and the percentage of *A*-*B* bonds dramatically increases. As the formation of one *A*-*B* bond in an island leads to the destruction of one *A*-*A* and one *B*-*B* bonds, and as the number of *B*-*B* bonds is twice less than *A*-*A* bonds, the mixing leads to a loss of *B*-*B* bonds approximately two times greater than *A*-*A* bonds. The occurrence of mixing is then shown by very different slopes of *A*-*A* and $2 \times B$-*B* curves [Fig. 3(b)]. In the same range of temperature, both the increasing mean size of the islands and smoothening of their edges result in a decrease in the perimeter over surface ratio and then in a slow increase in the number of bonds [Fig. 3(a)]. At even higher $T$, the number of bonds continues to increase with the mean island size, while the percentages reach a constant limit as the two species become totally alloyed.

To understand the influence of the flux upon the ring morphologies, the flux was varied from $F$=0.001 to 1 ML s$^{-1}$. A ring morphology similar to the one represented in Fig. 2(b) at

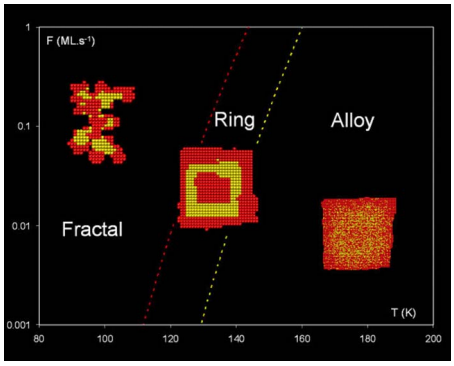


FIG. 4. (Color online) Temperature and/or flux diagram defining the morphology of the islands obtained by successive deposition of 0.05 ML of *A*, 0.10 ML of *B*, and 0.15 ML of *A*. The broken curves correspond to the transitions between the various morphologies.

$T$=120 K is obtained for a flux of 0.4 ML s$^{-1}$ at $T$=135 K, while that of Fig. 2(d) at $T$=150 K corresponds to a flux equal to 0.001 ML s$^{-1}$ at $T$=135 K. This can be interpreted in terms of the competition between the different processes involved. Indeed, rings need regular island edges during the whole growth, which is provided either by a temperature increase which favors reorganization around islands, or by a flux lowering that provides enough time to the island edges to relax. In the same way, mixing occurs either when it is thermally activated or when the flux is lowered enough to increase the deposition time. Thus, an increase of 15 K corresponds to a flux lowering by a factor of 20.

An exhaustive set of simulations was driven, in which $T$ was varied from 80 to 200 K and F from 0.001 to 1 ML s$^{-1}$. As the island morphology progressively changes, we had to make a choice concerning the borders of the shapely rings. The lower transition was decided to be the morphology obtained at $T$=125 K and $F$=0.02 ML s$^{-1}$, which is halfway between those represented in Figs. 3(a) and 3(b). The upper transition between rings and alloyed structures was chosen to correspond to the morphology obtained for the same flux at $T$=140 K [Fig. 3(c)]. Figure 4 displays the regions assigned to fractal-like, ringed, and alloyed islands in a flux-temperature diagram. We find rings in a narrow band, fractal shapes occurring at lower $T$ and/or higher $F$, and alloyed islands at higher $T$ and/or lower $F$. At the left hand border, the ratio of the flux over the diffusion rate along a straight island edge (with a barrier of 0.3 eV) is nearly constant and equal to $\alpha \approx 1.6 \times 10^{-2}$. This means that about 60 reorganization diffusions are required each time one atom is deposited upon the surface to obtain regular island edges and thus regular rings. This border follows the equation

$$F = \alpha \nu_0 \exp[-(E_D + E_L)/k_B T]. \quad (3)$$

At the right hand border, a value $\beta \approx 1.9$ of the ratio of the flux over the mixing rate is observed, which prevents the system from intermixing. This means that the mixing events must be twice less rapid than the deposition events. The right border in Fig. 4 obeys to the equation

$$F = \beta \nu_0 \exp(-E_M/k_B T). \quad (4)$$

The existence of rings is thus a subtle process which results in a double competition between flux and edge diffusion on the one hand and between flux and mixing on the other hand.

It may be noted that, in the present model, the rate of some processes is underestimated. As an example, edge diffusion, kink, and corner rounding seldom occur since diffusion and detachment have the same probability, thus limiting the island shape reorganization. However, favoring edge diffusion against detachment would lead to a shift to the left hand side of the fractal-to-compact transition in Fig. 4 only.

Although this discussion deals with a small set of parameters, it is fundamental in understanding the competition between the involved processes. Additional calculations have then been performed to analyze the influence of the various parameters. First, when physical systems display different diffusion barriers for $A$ and $B$, we can change deposition conditions by tuning $F$ and $T$ to provide comparable diffusion length for the two species. This approach was used by Kawamura *et al.*[7] and Voigtländer *et al.*[25] in their experiments to account for the different diffusion properties of Si and Ge. Second, the value of the mixing barrier $E_M(0)$ is also important. The lower it is, the more the right border of the ring zone [Fig. 4] moves toward the left, and its slope is lowered (Eq. (4)). A value $E_M(0)=1.85E_D(0)$ (instead of 2) lowers the border by 10 K, and $E_M(0)=1.75E_D(0)$ leads to total vanishing of the ring zone. It may be mentioned that with the chosen set of parameters, edge reorganization and lateral mixing have the same probability. As a consequence, regular shapes are obtained in the same conditions as fully intermixed islands. Increasing intermixing barrier could provide conditions for obtaining regular rings in equilibrium shape island. The left border of this zone is strongly influenced by $E_L$. Large values inhibit diffusion along island edge and displace this border toward the right, and its slope is increased [Eq. (3)]. A value $E_L=0.6E_D(0)$ (instead of 0.5) is sufficient to move it by 10 K, while $E_L=0.7E_D(0)$ prevents obtaining rings. Third, when the lateral energies are different, an increase in $E_{AA}$ or $E_{BB}$ favors the compactness of $A$ or $B$ zones and then prevents intermixing. On the contrary, an increase in $E_{AB}$ favors mixing, since atoms are more stable when surrounded by atoms of the other species. Such an effect is equivalent to decrease $E_M(0)$ by the same value. Note that, in order to limit the set of parameters, the intermixing with substrate atoms has been disregarded. If more efficient than lateral intermixing, such an additional process would still reduce the occurrence of perfect rings.

To conclude, we have conducted simulations on the nanoringed self-organization to demonstrate that the conditions required to form controlled rings are quite drastic. Since their occurrence range is narrowed both by edge diffusion and intermixing, it is not surprising to have found, up to date, very few examples in experiments. However, we have shown that they can appear in simple situations. The influence of stresses connected to the presence of a surfactant, which are able to promote the formation of rings, would require the consideration of additional parameters.


[1] A. V. Baranov *et al.*, Phys. Rev. B **73**, 075322 (2006).
[2] M. Larsson *et al.*, Phys. Rev. B **73**, 195319 (2006).
[3] C. Lang, S. Kodambaka, F. M. Ross, and D. J. H. Cockayne, Phys. Rev. Lett. **97**, 226104 (2006).
[4] J. T. Robinson *et al.*, Phys. Rev. Lett. **98**, 106102 (2007).
[5] M. Stoffel *et al.*, Phys. Rev. B **75**, 113307 (2007).
[6] N. Motta *et al.*, Phys. Rev. B **75**, 035337 (2007).
[7] M. Kawamura, N. Paul, V. Cherepanov, and B. Voigtländer, Phys. Rev. Lett. **91**, 096102 (2003).
[8] K. Romanyuk *et al.*, Phys. Rev. B **75**, 241309(R) (2007).
[9] P. Šmilauer and D. D. Vvedensky, Phys. Rev. B **48**, 17603 (1993).
[10] M. Kotrla, J. Krug, and P. Šmilauer, Phys. Rev. B **62**, 2889 (2000).
[11] R. J. Wagner and E. Gulari, Phys. Rev. B **69**, 195312 (2004).
[12] G. Katsaros *et al.*, Phys. Rev. B **72**, 195320 (2005).
[13] G. Hadjisavvas and P. C. Kelires, Phys. Rev. B **72**, 075334 (2005).
[14] T. Volkmann, F. Much, M. Biehl, and M. Kotrla, Surf. Sci. **586**, 157 (2005).
[15] J. A. Venables, J. DeGraffenreid, D. Kay, and P. Yang, Phys. Rev. B **74**, 075412 (2006).
[16] M. Einax, S. Ziehm, W. Dieterich, and P. Maass, Phys. Rev. Lett. **99**, 016106 (2007).
[17] Y. Tu and J. Tersoff, Phys. Rev. Lett. **98**, 096103 (2007).
[18] T. Ono and K. Hirose, Phys. Rev. Lett. **98**, 026804 (2007).
[19] A. F. van Driel *et al.*, Phys. Rev. Lett. **95**, 236804 (2005).
[20] T.-Y. Lee, S. Sarbach, K. Kuhnke, and K. Kern, Surf. Sci. **600**, 3266 (2006).
[21] D. Kandel and E. Kaxiras, Solid State Phys. **54**, 219 (2000).
[22] S. N. Filimonov *et al.*, Surf. Sci. **599**, 76 (2005).
[23] V. Cherepanov, S. Filimonov, J. Mysliveček, and B. Voigtländer, Phys. Rev. B **70**, 085401 (2004).
[24] N. Paul, H. Asaoka, J. Mysliveček, and B. Voigtländer, Phys. Rev. B **69**, 193402 (2004).
[25] B. Voigtländer, M. Kawamura, N. Paul, and V. Cherepanov, Thin Solid Films **464-465**, 185 (2004).
[26] A. Voigt, *Multiscale Modeling in Epitaxial Growth*, *International Series of Numerical Mathematics*, Vol. 149 (Birkhauser, Basel, 2006).
[27] P. Politi, G. Grenet, A. Marty, A. Ponchet, and J. Villain, Phys. Rep. **324**, 271 (2000).
[28] C. Ratsch, M. C. Wheeler, and M. F. Gyure, Phys. Rev. B **62**, 12636 (2000).
[29] M. Biehl, M. Ahr, W. Kinzel, and F. Much, Thin Solid Films **428**, 52 (2003).
[30] C. Ratsch, P. Šmilauer, D. Vvedensky, and A. Zangwill, J. Phys. I **6**, 575 (1996).
[31] C. H. Lam, C. K. Lee, and L. M. Sander, Phys. Rev. Lett. **89**, 216102 (2002), and references quoted therein.
[32] G. Russo and P. Smereka, J. Comp. Physiol. **214**, 809 (2006), and references quoted therein.
[33] P. Šmilauer, K. Mizushima, and D. D. Vvedensky, Phys. Rev. Lett. **81**, 5600 (1998).
[34] J. G. Amar and F. Family, Thin Solid Films **272**, 208 (1996).
[35] J. W. Evans and M. C. Bartelt, Phys. Rev. B **63**, 235408 (2001).
[36] G. S. Bales and D. C. Chrzan, Phys. Rev. Lett. **74**, 4879 (1995).